Manuscript prepared for Geosci. Model Dev. Discuss.
with version 4.1 of the LaTeX class copernicus_discussions.cls.
Date: 19 August 2014

Implementation of a soil albedo scheme in the CABLEv1.4b land surface model and evaluation against MODIS estimates over Australia

Jatin Kala[1], **Jason P. Evans**[1], **Andy J. Pitman**[1], **Crystal B. Schaaf**[2], **Mark Decker**[1], **Claire Carouge**[1], **David Mocko**[3], **and Qingsong Sun**[2]

[1]Australian Research Council Centre of Excellence for Climate Systems Science and Climate Change Research Centre, University of New South Wales, Sydney, NSW, 2052, Australia
[3]SAIC at NASA Goddard Space Flight Centre, NASA, Greenbelt, MD, USA
[2]Department of Earth and the Environment, Boston University, Boston, Massachusetts, USA

Correspondence to: Jatin Kala
(J.Kala@unsw.edu.au or Jatin.Kala.JK@gmail.com)

Abstract

Land surface albedo, the fraction of incoming solar radiation reflected by the land surface, is a key component of the earth system. This study evaluates snow-free surface albedo simulations by the Community Atmosphere Biosphere Land Exchange (CABLEv1.4b) model with the Moderate Resolution Imaging Spectroradiometer (MODIS) and the Satellite Pour L'Observation de la Terre (SPOT) albedo. We compare results from offline simulations over the Australian continent. The control simulation has prescribed background snow-free and vegetation-free soil albedo derived from MODIS whilst the experiments use a simple parameterisation based on soil moisture and colour, originally from the Biosphere Atmosphere Transfer Scheme (BATS), and adopted in the Community Land Model (CLM). The control simulation, with prescribed soil albedo, shows that CABLE simulates overall albedo over Australia reasonably well, with differences compared to MODIS and SPOT albedo within $\pm$ 0.1. Application of the original BATS scheme, which uses an 8-class soil classification, resulted in large differences of up to -0.25 for the near infra-red (NIR) albedo over large parts of the desert regions of central Australia. Use of a re-calibrated 20-class soil colour classification from the CLM, which includes a higher range for saturated and VIS and NIR soil albedos, reduced the under-estimation of the NIR albedo. However, this soil colour mapping is tuned to CLM soil moisture, a quantity which is not necessarily transferrable between land surface models. We therefore re-calibrated using CABLE's climatological soil moisture, which further reduced the under-estimation of the NIR albedo to within $\pm$ 0.15 over most of the continent as compared to MODIS and SPOT albedo. Small areas of larger differences of up to -0.25 remained within the central arid parts of the continent during summer, however, the spatial extent of these large differences is substantially reduced as compared to the simulation using the default 8-class un-calibrated soil colour map. It is now possible to use CABLE coupled to atmospheric models to investigate soil moisture-albedo feedbacks, an important enhancement to the model.

1 Introduction

The albedo of the land surface is the ratio of upwelling to downwelling shortwave radiation and determines the fraction of incoming solar radiation reflected back to the atmosphere. It is one of the key drivers of the earth's climate as it determines, in part, the amount of energy available to drive processes in the atmosphere and the land surface (e.g., Dickinson, 1983). The incorrect prescription or parameterisation of surface albedo can result in large model biases. Therefore, the correct representation of albedo in land surface models (LSMs), whether prescribed or parameterised, is of critical importance to the surface energy and hydrological cycle.

The overall albedo of the land is a function of the vegetation, soil, and snow albedos. The main factor which determines which of these three albedos has the strongest influence on the overall surface albedo is the fractional area covered by each of vegetation, soil and snow. These are commonly parameterised as a function of leaf area index (LAI), the total one-sided surface area of leaf per ground surface area (Bonan, 2008). When LAI is high, most of the incoming solar energy is reflected, scattered, and/or absorbed by the vegetation canopy and only a small proportion of radiation reaches the ground and the overall albedo is primarily that of the vegetation canopy. When LAI is small, the converse is true and the overall albedo is increasingly represented by the albedo of the soil or snow.

Vegetation albedo is a function of the radiative properties of the canopy. These properties include the leaf transmittance and reflectance, leaf angle or orientation, canopy clumping, and structure. Leaf transmittance and reflective properties determine how much radiation penetrates through the canopy and are usually prescribed in LSMs for each plant functional type (PFT) in the visible (VIS, 0.4-0.7 μm) and near infra-red (NIR, 0.7-4.0 μm) bands. This distinction is important since green canopies absorb most of the solar radiation in the VIS waveband for photosynthesis, but reflect and transmit most of the radiation in the NIR waveband (Bonan, 2008). Leaf structural and physical properties can also influence within-canopy shadowing, which allows higher exposure of the underlying soil and/or snow cover, especially in low density forests (Davidson and Wang, 2004). Leaf orientation influences albedo since the maximum

incident solar radiation on a leaf occurs when the beam is perpendicular to the surface (Bonan, 2008).

Soil albedo is a function of soil colour, determined partly by organic composition and soil moisture, with saturated soils generally having lower albedo than dry soils (Idso et al., 1975). This is especially important in transitional climatic regions, where significant soil moisture variability drives strong land-atmosphere coupling (e.g., Koster et al., 2004). Although the dependence of soil albedo on soil moisture has been well established from field experiments (e.g., Idso et al., 1975), not all LSMs include this feedback and recent studies have shown that it plays in important role in seasonal droughts in the central US (Zaitchik et al., 2012). Recent studies over eastern Australia have shown that the use of time-varying MODIS albedo (as opposed to monthly mean climatologies from AVHRR) in a regional climate model improved mean air temperature simulations, and to a lesser extent, precipitation (Meng et al., 2013). This was particularly evident in arid regions where the overall albedo is predominantly influenced by soil rather than vegetation.

Vegetation and soil albedo are also influenced by the solar zenith angle, especially in desert regions (Wang et al., 2005). This only applies under clear-sky conditions (i.e., direct beam radiation) when there is little or no scattering of the incoming shortwave radiation. In the morning just after sunrise and late afternoon before sunset, albedo is generally higher, as compared to mid-day when the sun is directly overhead. The inclusion of soil and vegetation albedo dependence on solar zenith angle during clear-sky conditions has improved albedo simulations in some LSMs (Liang et al., 2005).

With recent developments in satellite remote sensing, several surface albedo products are now available at a high spatial and temporal resolution and spanning several years. This has allowed for the careful evaluation of albedo in various LSMs (e.g., Wei et al., 2001; Oleson et al., 2003; Zhou et al., 2003; Wang et al., 2004) and the development of vegetation and soil albedo parameterisations (e.g., Liang et al., 2005; Yang et al., 2008). These remotely sensed products have also allowed the mapping of land surface parameters such as the spatial and temporal distribution of PFTs, LAI and soil color, for use in LSMs (Lawrence and Chase, 2007). Clearly,

the use of satellite remote sensing can be very useful in both the evaluation and development of LSMs.

This paper focusses on the Community Atmosphere Biosphere Land Exchange (CABLE) model (Wang et al., 2011), an LSM designed to simulate fluxes of heat, moisture, and carbon at the land surface. While several studies have used CABLE (e.g., Cruz et al., 2010; Zhang et al., 2011; Pitman et al., 2011; Wang et al., 2012; Exbrayat et al., 2012), previous studies have not explicitly examined simulations of surface albedo. The aim of this paper is to address this key knowledge gap by comparing CABLE albedo simulations with remotely sensed albedo estimates to better quantify the uncertainties in CABLE's albedo parameterisation. Section 2 provides on overview of CABLE with detailed description of the parameterisation of surface albedo. This is followed by the experimental design and description of the satellite remote sensing products used to compare against CABLE albedo simulations. Results are presented in Section 3 and discussed in Section 4.

2 Methods

2.1 Model description

CABLE simulates fluxes of energy, water and carbon at the land surface and can be run as an offline-model with prescribed meteorology (e.g., Abramowitz et al., 2008; Wang et al., 2011; Kala et al., 2014) or fully coupled to an atmospheric model within a global (Mao et al., 2011; Lorenz et al., 2014) or regional context (Hirsch et al., 2014). CABLE is a key part of the Australian Community Climate Earth System Simulator (ACCESS, see http://www.accessimulator.org.au), a fully coupled earth system science model used in the Coupled Model Intercomparison Project Phase 5 (CMIP-5) . The version used in this study is CABLEv1.4b.

In CABLEv1.4b (Wang et al., 2011), the one-layered, two-leaf canopy radiation module of Wang and Leuning (1998) is used for sunlit and shaded leaves and the canopy micrometeorology module of Raupach (1994) is used for computing surface roughness length, zero-plane displacement height, and aerodynamic resistance. The model also consists of a surface

flux module to compute the sensible and latent heat flux from the canopy and soil, the ground heat flux, as well as net photosynthesis. A soil module is used for the transfer of heat and water within the soil and snow, and an ecosystem carbon module based on Dickinson et al. (1998) is used for the terrestrial carbon cycle. A detailed description of each of the modules can be found in Kowalczyk et al. (2006) and Wang et al. (2011).

Land albedo in CABLE is a function of the vegetation albedo, snow albedo, and the background snow-free and vegetation-free soil albedo (the fractional albedo of inland water surfaces was not considered in the simulations). The parameterisation of albedo is part of the canopy radiative transfer model. The latter accounts for direct beam and diffuse radiation separately, and within each stream, albedo is computed separately in the NIR and VIS wavebands as plants utilise energy differently in these two parts of the spectrum. Appendix A provides a detailed description of the albedo parameterisation and a schematic illustration is presented in Fig. 1.

The overall albedo of the surface (snow-free) is a function of the direct and diffuse effective reflectances and the fraction of direct beam shortwave radiation in the NIR and VIS wavebands (Eq. A1 and Figure 1). When running CABLE offline, the fraction of direct beam shortwave radiation is computed empirically from incoming shortwave radiation (meteorological input to the model), solar constant, julian day of year, and solar zenith angle, following Spitters (1986). When coupled, it is provided by the atmospheric radiation module. The direct and diffuse effective reflectances are a function of the canopy reflectance and extinction coefficients for direct and diffuse radiation, the soil reflectance, and LAI (see Eqs. A2 and A3 and Figure 1). In CABLEv1.4b, LAI is prescribed as the model does not include a dynamic vegetation model or dynamic phenology. The soil reflectance is derived from the prescribed background snow and vegetation-free soil albedo.

The canopy reflectance for direct radiation is a function of the direct and diffuse extinction coefficients for a black canopy and the reflectance of a homogenous canopy with horizontal black leaves (Eq. A4). The canopy reflectance for diffuse radiation is in turn dependent on the canopy reflectance for direct radiation, and the solar zenith angle (Eq. A5). The extinction coefficients for direct and diffuse radiation are a function of the corresponding extinction coefficients for a black canopy, and the leaf transmittance and reflectance (Eq. A6). The direct and diffuse ex-

tinction coefficients for a black canopy are a function of solar zenith angle, LAI, and leaf angle (Eq. A7 to A11). Finally, the reflectance of a horizontal homogeneous canopy with horizontal black leaves is also a function of the leaf radiative properties (Eq. A12). In summary, the albedo parameterisation in CABLE is reasonably complex, as illustrated in Figure 1. User-defined input parameters which influence albedo are the LAI, background snow and vegetation-free soil albedo, leaf angle, and the leaf transmittance and reflectance.

While it is common to prescribe LAI and leaf physical and radiative properties in most LSMs, several LSMs include simple parameterisations for the background snow and vegetation-free soil albedo based on soil moisture content. Since this soil moisture-albedo feedback has been shown to be important (e.g., Vamborg et al., 2011; Zaitchik et al., 2012), we added a simple parameterisation based on soil colour and moisture, originally developed for the Biosphere-Atmosphere Transfer Scheme (BATS) LSM (Dickinson et al., 1993), and adopted by the Common Land Model (CLM) (Zhou et al., 2003):

$$\alpha_{soil} = \alpha_{sat} + \min\{\alpha_{sat}, \max[0.11(11 - 40\theta_{sm}), \alpha_{dry}]\} \quad (1)$$

Where α_{sat} and α_{dry} are the albedo of saturated and dry soils respectively, dependent on the soil colour (light to dark, see Table 1) and θ_{sm} is the surface volumetric soil moisture content. The saturated and dry soil albedos in the VIS waveband as shown in Table 1 are simply assumed to be twice those in the NIR waveband. As noted by Wang et al. (2004), this assumption is not un-reasonable, although some studies have shown this ratio varies geographically (Tsvetsinskaya et al., 2002).

2.2 Simulations

CABLEv1.4b was used within the NASA Land Information System (LIS-6.1) (Kumar et al., 2006, 2008), a flexible software platform designed as a land surface modelling and hydrological data assimilation system. A grid resolution of $0.25^{o} \times 0.25^{o}$ was utilised, covering continental Australia. Our domain is shown in Fig. 2 (a) which also illustrates the distribution of PFTs used (Table 2). The model was forced with the Modern Era Retrospective-analysis for

Research and Applications (MERRA) reanalysis (Rienecker et al., 2011) at 3-hourly intervals from 2001-2008 and initialised from a previous 30-year spin-up. This year range was chosen as it corresponded with the availability of the remotely sensed albedo products. The forcing variables included incoming long-wave and shortwave radiation, air temperature, specific humidity, surface pressure, wind speed and precipitation. The MERRA reanalysis was bias-corrected for precipitation using the Australian Bureau of Meteorology Australian Water Availability gridded precipitation dataset (Jones et al., 2009), following Decker et al. (2012). A monthly mean MODIS derived LAI climatology from Yuan et al. (2011) was used for the simulations as shown in Fig. 3. Although monthly mean values are used in the simulations, we show seasonal means in Fig. 3 to help the interpretation of seasonal differences in albedo in Section 3. Monthly ambient carbon dioxide concentrations were prescribed using measurements from Baring Head, New Zealand (Keeling et al., 2005). Outputs were saved every hour, for the direct and combined (direct and diffuse) albedos, in the VIS and NIR wavebands respectively.

As discussed in Section 2.1, in CABLEv1.4b, the background snow-free and vegetation-free soil albedo are prescribed by default. We used the MODIS derived vegetation and snow-free background soil albedo data from Houldcroft et al. (2009) shown in Fig. 2 (b). In this data-set, bare soil regions, as defined by the IGBP land-use classification map which was also used in CABLE, are assigned the mean albedo over the data period (October 2002 to December 2006), while partially vegetated pixels are assigned a soil albedo derived from a linear relationship between albedo and the Normalised Difference Vegetation Index (NDVI). A linear regression model is then used to estimate the background soil albedo corresponding to zero LAI (Houldcroft et al., 2009). This simulation was the control (CNTL) experiment. An additional simulation was also carried out with the background snow and vegetation-free albedo parameterised using Eq. 1, hereafter referred to as experiment PSALB (where PSALB is referring to Parametrized (P) Soil (S) Albedo(ALB)). The spatial distribution of soil colours for the PSALB experiment is shown in Fig. 2 (c). For both the CNTL and PSALB simulations, leaf transmittance and reflectance properties and leaf angles were prescribed for each PFT following previous studies using CABLE (Pitman et al., 2011; Avila et al., 2012).

Sample model namelist files for the CNTL and PSALB experiments are available online at: https://bitbucket.org/jkala/gmd-2014-9/src.

2.3 MODIS albedo

The albedo products from MODIS have been extensively used for the purpose of evaluating albedo from various LSMs (Oleson et al., 2003; Zhou et al., 2003; Wang et al., 2004). In this study, we used the MODIS MCD43GF 30 arc-seconds gap-filled snow-free albedo product (available at: http://www.umb.edu/spectralmass/terra_aqua_modis/modis_brdf_albedo_cmg_gap_filled_snow_free_product_mcd43gf_v005). The MCD43D product utilizes directional reflectances from both the Aqua and Terra MODIS instruments to retrieve an appropriate surface anisotropy model and thus intrinsic measures of surface albedo (Lucht et al., 2000; Schaaf et al., 2002; Wang et al., 2004). The MCD43 product is validated to stage-3 signifying that the high quality retrievals are within 5% of field measurements. Additionally, a very recent field evaluation of the MCD43A product (from which the MCD43D is derived) found root mean square errors of less than 0.03 over over agricultural and grassland sites, and less than 0.02 over forested sites, during dormant snow-free periods (Wang et al., 2014). To avoid interpreting results that are within observational uncertainty, we only show differences between MODIS and simulated albedo which are greater than 0.05. The MCD43D product also provides data quality flags for each grid cell, and approximately 75% of grid-cells over the domain of interest were classified as high-quality (flags 0 and 1), and 25% were temporally fitted (flag 2). These temporally fitted points were mostly confined north of 20^{o}S, i.e., the northern tropical regions where cloud fraction is generally high.

To enable comparison with the simulations, the MODIS albedo products were interpolated to the grid domain used for the simulations. Following previous studies (Oleson et al., 2003; Zhou et al., 2003; Wang et al., 2004), we compared the CABLE simulated direct beam VIS and NIR albedos at local solar noon (obtained by combining the appropriate longitude bands from hourly outputs) to the VIS and NIR black-sky albedos from MODIS. The MCD43 product retrieval is attempted every 8 days over 16 days of potential input. We computed means of the local solar noon direct VIS and NIR direct-beam albedos from CABLE over the same time-

interval of data availability to enable more meaningful comparisons. The CABLE combined (direct and diffuse) VIS and NIR albedos were compared against the MODIS blue-sky VIS and NIR albedos. The MODIS blue-sky albedo represents both the diffuse and direct radiation and uses MODIS aerosol optical depth (the MOD04 product) where available or 0.2 as a mean climatology where unavailable. The blue sky-albedo used here is also valid at local solar noon, and hence is compared with the CABLE combined VIS and NIR albedos at the same time.

2.4 SPOT albedo

Given that the prescribed soil albedo for the CNTL experiment is MODIS-derived, we face the issue that the CNTL and benchmarking data-set are from the same source. Hence, we also use an alternative remotely sensed albedo data-set, the Satellite Pour L'Observation de la Terre (SPOT) albedo product (Lacaze et al., 2012). This dataset comprises of a black and white-sky albedo at a 10-day frequency and resolution of 1/112 of a degree (approximately 0.89 km). The SPOT product has not under-gone as extensive field evaluation as MODIS albedo, however, it is considered to be of comparable quality to MODIS (Lacaze et al., 2012). Disney et al. (2004) compared MODIS and SPOT albedo to field observations over an agricultural site in the UK, and found MODIS and SPOT albedo to correspond well. They found that SPOT albedo tends to vary more smoothly than MODIS albedo due to the SPOT product being derived over a longer averaging window, whereas the MODIS data is processed over shorter time-blocks. Since there is no equivalent post-processed blue-sky SPOT albedo product comparable to the MODIS blue-sky product, we only used the SPOT VIS and NIR black-sky product to compare against the CABLE simulated direct beam VIS and NIR albedo at local solar noon. A comparison between MODIS and SPOT VIS and NIR black-sky albedo is shown in Fig. 4. The main difference between the two products is that the MODIS product has slightly higher NIR albedo during JJA (winter) over central and southwest Australia and slightly lower albedo over the forests of eastern Australia and the northern savannah during summer (DJF) and autumn (MAM).

2.5 AMSR-E soil moisture

Given the dependance of the soil albedo parameterisation on soil moisture, it is useful to quantify the uncertainties in the simulated soil moisture. Given the lack of in-situ soil moisture observations, we used satellite derived soil moisture from the Advanced Microwave Scanning Radiometer-Earth Observing System (AMSR-E), which uses brightness temperatures to derive surface soil moisture. The version of the AMSR-E data used in this study is described in Liu et al. (2009) and available from July 2002 onwards. Hence we only use data over the period 2003 to 2008.

In summary, the CNTL simulation uses prescribed soil albedo and the PSALB experiment parameterises soil albedo based on Eq. 1. Both simulations are compared against MODIS and SPOT albedo estimates, and we use AMSR-E soil moisture as means of quantifying the uncertainties in CABLE soil moisture. An initial analysis of the differences between CABLE and MODIS and SPOT albedo showed that most of the differences greater than $\pm$ 0.05 were statistically significant at 95%. Hence, we simply show the absolute differences. In this context, deviations of more than 0.1-0.2 from remotely sensed estimates are considered to be large enough to warrant further improvements to the model.

3 Results

Figures 5 and 6 show the yearly and seasonal differences between CABLE and MODIS Blue-sky and black-sky NIR and VIS albedo and SPOT black-sky VIS and NIR albedo for the CNTL and PSALB experiments respectively (i.e., CNTL-MODIS and PSALB-MODIS respectively). Biases and root-mean-square-errors (RMSE) are shown in Tables 3 and 4 respectively, with RMSE and bias values scaled by 100 such that small differences are easier to see. The CNTL experiment (with prescribed soil albedo) shows that CABLE simulates albedo well (Fig. 5) when compared to both MODIS and SPOT albedo. The model has a systematic under-estimation of the Black-Sky NIR albedo, especially during DJF (summer) of around 0.1 and over-estimation

of the Blue-Sky VIS albedo for all seasons between 0.05 and 0.1. This over-estimation of Blue-Sky VIS albedo is over most of the interior continent which has low LAI (Fig. 3). This suggests that part of this bias may be inherited from the prescribed soil albedo used (Fig. 2b). However, the bias is also present in the northern tropical areas which have an LAI of 2.0 where vegetation should have a larger influence. The northern tropical regions is also where the MODIS albedo used for evaluation had higher percentages of temporally fitted data which might also contribute to these biases. We also note that that there is a consistent difference of 0.05 to 0.1 for the blue-sky NIR albedo in densely vegetated areas of Tasmania and the northern tropics. This has been documented elsewhere for other LSMs which use a similar two-stream radiation transfer scheme, as is used in CABLE. For example, Pinty et al. (2011) report that the lowering of the NIR leaf scattering coefficient below its true value was required to correct the absorption due to multiple scattering within a structurally heterogeneous canopy.

Figure 6 shows that the implementation of the soil albedo scheme resulted in similar differences to the CNTL experiment for the Black and Blue-Sky VIS albedos, but large differences of up to -0.25 for the Black and Blue-Sky NIR albedos. These large differences were confined to central Australia (shown by the black box in the Black Sky NIR yearly panel), which is the most arid part of the continent. The larger differences for the NIR as compared to the VIS albedos can be expected as NIR albedo is generally larger in magnitude as compared to VIS albedo. The fact that these differences are confined to inland arid regions suggests that the mechanisms leading to high albedo values in desert regions is not being adequately represented. Similar to CNTL, the PSALB experiment also showed larger differences during DJF (summer) as compared to the other seasons, noticeably in the northern tropical regions (also shown by a black box in the Black Sky NIR yearly panel). A monthly time series of the differences between PSALB and MODIS over the central and northern areas (Fig. 7) shows that PSALB consistently underpredicts the Black Sky NIR albedo during summer in the north (the monsoon season), whereas the differences in the central arid region show little monthly variation. The CNTL experiment showed similar consistent underestimation of Black Sky NIR albedo for the northern tropical region, suggesting that these differences are related to the parameterisation of vegetation, rather than soil albedo.

The soil albedo scheme implemented depends on soil colour, which is prescribed (Fig. 2(c)) and soil moisture. To examine the uncertainties in the simulated soil moisture, we compared yearly and seasonal means of soil moisture from the PSALB experiment against AMSR-E satellite estimated surface soil moisture. CABLE's surface soil moisture is representative of the first 2.2 cm of the soil, and details of the numerical scheme used to solve the 1-Dimensional Richard's equation can be found in Kowalczyk et al. (2006). While comparing an LSM soil moisture to a satellite derived product is not strictly comparing like-to-like, our goal here is to identify whether there are any spatial similarities in the differences between CABLE albedo and soil moisture from satellite derived alternatives, rather than examine the absolute soil moisture values. CABLE's soil moisture is generally higher compared to AMSR-E for most of the continent (Fig. 8), especially during DJF and SON. Higher soil moisture should result in lower simulated soil albedo and hence larger differences as compared to MODIS. Hence this could partly explain the large deviations in the NIR albedo.

To further quantify the contribution of the uncertainties in CABLE simulated soil moisture on albedo, we computed the correlation between the monthly mean differences in CABLE surface soil moisture and AMSR_E soil moisture, and CABLE Black-Sky NIR albedo and MODIS and SPOT estimates. This is shown in Figs. 9 (a) and (b) respectively. The correlations were computed over the period 2003-2008 (we did not compute correlations at the yearly and seasonal time-scales as the time-series was too short) and results shown are at the 95% level. A negative correlation shows that an over-estimation of soil moisture (i.e., +ve difference between CABLE and AMSR_E) is correlated with an under-estimation in albedo (i.e., -ve difference between CABLE and remotely sensed (MODIS and SPOT) Black-Sky NIR albedo). Large parts of the centre of the continent showed a negative correlation, with SPOT albedo showing larger and more statistically significant correlations as compared to MODIS. Hence, at least part of the large differences in the Black-Sky NIR albedo over the centre of the continent can be attributed to CABLE over-estimating soil moisture.

Figure 10 shows the difference in overall albedo and surface fluxes between the PSALB and CNTL experiments (PSALB-CNTL). The lower albedo values in central Australia for the PSALB experiment result in an increase in net radiation of up to 45-50 W m^{-2}, most of which

results in increased sensible heat because the continental interior is generally dry. The only noticeable change in latent heat is during the summer monsoon season (DJF) over the Northern tropical regions, when high precipitation leads to higher available soil water. Also illustrated in Fig. 10 is a diagnostic screen temperature showing the lower albedo and higher net radiation and sensible heat for the PSALB experiment leading to higher temperature by up to 0.5°C.

Such large deviations from MODIS albedo with this simple parameterization have also been noted with the CLM LSM. To reduce these deviations, Lawrence and Chase (2007) extended the 8-soil colour class to 20 colours to include a higher range of VIS and NIR albedos as observed from MODIS. They also generated a new MODIS consistent soil colour map by fitting VIS and NIR soil albedos which reproduced the MODIS monthly values at local solar noon as closely as possible, given a model climatological monthly mean soil moisture. Hence, we implemented the 20-class soil colour map used by Lawrence and Chase (2007) and undertook a similar re-calibration using CABLE's soil moisture. The CLM and CABLE calibrated soil colour maps are shown in Fig. 11 (a) and (b) respectively, and the corresponding saturated and dry VIS and NIR albedos are shown in Table 5. The new soil colour maps clearly better reflect the spatial distribution of MODIS soil albedo as compared to the default 8-class map (Fig. 2).

Figure 12 shows the differences in albedo between CABLE with the 20-class CLM calibrated soil colour map (Fig. 11) (experiment PSALB_20) and MODIS as well as the difference against SPOT. The domain averaged bias and RMSEs are shown in Table 6. The large differences in the black-sky and blue-sky NIR albedo in central Australia (Fig. 12) are clearly reduced. Comparisons with the SPOT product show a larger reduction compared to MODIS for the black-Sky NIR albedo, which is related to MODIS having slightly higher NIR albedo as compared to SPOT (Fig. 4). The over-estimation of the Blue-sky VIS albedo is also reduced. However, we note that although the differences in black-sky NIR albedo in the centre of the continent is reduced, differences in the black-sky NIR albedo increase by 0.05 to 0.1 to the west and north of the continent as compared to the PSALB experiment (Fig. 6). Hence the domain averaged statistics shown in Table 6 do not show a marked improvement as compared to the PSALB experiment (Table 4). The differences in overall broadband albedo (combined VIS and NIR, direct and diffuse albedo, averaged at all model times), heat fluxes, and diagnostic screen temperature

between the PSALB_20 and CNTL experiment is shown in Fig. 13. The differences in the centre of the continent are not as large as compared to the PSALB experiment (Fig. 10), but overall albedo is generally under-estimated as compared to the CNTL.

Using a colour map which is re-calibrated to CABLE soil moisture (Fig. 11 (b)) (experiment PSALB_20C) reduces the difference in NIR albedo in centre of the continent further (Fig. 14), but the systematic under-estimation of the local-noon black-sky NIR albedo of 0.05-0.15 as compared to MODIS and SPOT over most of the continent remains, with the largest differences being in summer (DJF). The difference in dry and saturated albedo between each successive soil colour class (Table 5) is 0.01-0.02, hence such differences are within the expected range. Although the differences with MODIS and SPOT are largely reduced as compared to the PSALB experiment (Fig. 6), relatively small areas with differences of up -0.20 in the centre of the continent remain. This suggests an inherent limitation of this parameterisation in soil albedo in very arid regions. The domain averaged statistics are illustrated in Table 7, showing an improvement as compared to the PSALB (Table 4). The differences in overall albedo, heat fluxes, and diagnostic screen temperature as compared to the CNTL are shown in Fig. 15. These differences are now small enough to enable use of the scheme to explore soil-moisture albedo feedbacks within CABLE.

4 Discussion

CABLE traditionally prescribes background soil albedo and hence does not allow for soil moisture-albedo feedbacks, which the literature suggests can be important. To address this issue, we implemented a simple soil albedo scheme, based on soil moisture and colour, which has been used in other LSMs. Two simulations were conducted, one with prescribed soil albedo derived from MODIS, the control (CNTL) experiment, and another with parameterised soil albedo (PSALB). The CNTL simulation showed relatively small differences in albedo when compared to MODIS and SPOT albedo whereas the PSALB experiment showed much larger differences, especially in the VIS albedo. The differences were up to -0.25 and mainly in central Australia. The better performance of the CNTL as compared to PSALB is not surprising as the CNTL ex-

periment uses a background soil albedo which is itself derived from earlier versions of MODIS albedo (Houldcroft et al., 2009). The equally small differences when compared to an alternative remotely sensed albedo product, SPOT, gives us confidence that the small differences are not simply due to CNTL soil albedo and the benchmarking data-set being from the same source.

The large differences in the NIR albedo in the desert regions of Australia has been found elsewhere. Wang et al. (2004) compared albedo simulations globally from the CLM2 LSM against MODIS and also found similar large differences in the NIR albedo in central Australia (see Fig. 5(c) in Wang et al. (2004)). Other studies have also found that the largest differences in NIR albedo from LSMs tend to be in desert and arid regions such as the Sahara (Wei et al., 2001; Oleson et al., 2003; Zhou et al., 2003; Wang et al., 2004). The much larger differences for the NIR as compared to the VIS albedo as found in this study has also been reported by Wang et al. (2004). This is partly due to the fact that NIR albedos over snow-free surfaces are larger in magnitude than the VIS albedo, and hence, likely to show larger differences.

Given the large differences in albedo between MODIS and LSMs, Lawrence and Chase (2007) developed MODIS-consistent land-surface parameters, including the mapping of PFTs, LAI, and soil color for use within the CLM3 LSM. They demonstrated that the use of the modified parameter maps improved surface albedo simulations when compared with MODIS albedo. In some instances, this resulted in improved simulations of precipitation and near-surface temperature. We therefore carried out a similar procedure and tested the modified CLM calibrated soil colour map of Lawrence and Chase (2007). We also carried out a similar calibration using CABLE climatological soil moisture. Use of these maps resulted in a reduction in the difference in the NIR albedo in central Australia as compared to MODIS and SPOT estimates, with the CABLE calibrated map resulting in smaller differences as compared to the CLM calibrated map. Comparisons with the CNTL overall albedo and heat fluxes showed differences which were small enough to warrant use of the new scheme in CABLE to further explore soil-moisture albedo feedbacks.

The use of re-calibrated maps, whilst reducing the difference between CABLE and MODIS and SPOT estimates, did not completely fix the issue of underestimation of the local-noon black-sky NIR albedo as there were still small areas in central Australia whereby differences in the

local noon NIR black-sky albedo were up to approximately -0.2. There may be several reasons for this. Firstly, as was shown in Fig. 9, at least part of the large differences in the NIR albedo can be attributed to CABLE over-estimating surface soil moisture, and hence simulating lower albedo. Secondly, the parameterisation and coefficients in Eq. 1 were originally developed for the BATS LSM (Dickinson et al., 1993), subsequently adopted in CLM, and now in CABLE. Eq. 1 is based on an absolute soil moisture value and this presents issues with regards to the universal application of the scheme irrespective of LSM, as the latter vary considerably in their treatment of soil moisture (Koster et al., 2009), as well as the processes which influence soil moisture (Koster and Milly, 1997). Whilst we re-calibrated the soil colour maps, we have not re-calibrated the coefficients used in Eq. 1 as this formulation was designed such that the soil albedos range in a nonlinear manner between their saturated and dry values (Dickinson et al., 1993). Rather than altering the formulation, we choose to re-calibrate the soil colour maps. Additionally, it is assumed that the ratio of the NIR to VIS albedo is exactly a factor of 2. However, Wang et al. (2005) have shown that this ratio from MODIS data over the arid part of central Australia is 2.69. We could make use of a higher factor and this would help over Australia, but it would also lead to larger differences elsewhere in global simulations.

One cause of the large differences between LSM simulated and observed albedo in arid regions is the dependence of soil albedo on solar zenith angle (Wang et al., 2005; Yang et al., 2008), and the lack of an explicit physical representation of this relationship in many LSMs. Wang et al. (2005) devised a semi-empirical scheme to relate bare soil albedo at a single site in the Sahel to solar zenith angle, and show improvements in albedo and surface flux simulations when applied to the NOAH land surface model. However, their simulations were at the site-scale, and over a very short time-frame (less than 2 months) and may not be easily applicable to regional or global simulations over longer time-frames. Liang et al. (2005) developed a "dynamic-statistical" parameterisation of snow-free albedo using MODIS albedo and soil moisture from a land data assimilation system over North America. While the dynamical part of the model represents the physical dependencies on solar zenith angle and surface soil moisture etc., the statistical model provides parameter estimates specific to geographic location. This scheme has been shown to significantly improve albedo simulations in CLM over North America, but

a globally applicable scheme is yet to be trialled. Hence, we identify this an important future direction for albedo parameterisation development in CABLE.

5 Conclusions

Surface albedo is a key element of the surface energy balance as it determines the amount of solar energy absorbed at the surface and re-distributed into sensible and latent heat, which in turn drive the surface energy and water cycles. In this study, we investigated how well CABLEv1.4b simulates albedo compared with MODIS and SPOT estimates. We also tested a new simple parameterisation for the soil albedo, which is prescribed and held constant in time in the standard version of CABLE. This is an important step for the model as it enables the feedback between albedo and soil moisture to be represented. Our results show that CABLEv1.4b simulates overall albedo reasonably well when the soil albedo is prescribed as would be expected. The new parameterisation for soil albedo, after calibration to produce a MODIS consistent soil colour map, which is also tuned to CABLE soil moisture, resulted in satisfactory comparisons with both MODIS derived albedo, and an alternative remotely sensed albedo product, SPOT. Hence, there is now added capacity and value within CABLE to further explore soil-moisture albedo feedbacks.

Our results also highlight the issue of parameterisations which are based on soil moisture, a quantity which is not interchangeable between LSMs. Hence, a process of re-calibration is required as this can have significant impacts on the surface energy balance. The re-calibration carried out for this study may need to be repeated if future model developments have a significant influence on soil moisture. Given the availability of MODIS and SPOT albedo products, we therefore argue that the evaluation of LSM simulated albedo is an important part of any standard model evaluation and/or benchmarking protocol. This should ideally be adopted across the LSM community.

Appendix A

Parameterisation of surface albedo in CABLEv1.4b

The overall albedo of the land surface for shortwave radiation (α_s) is defined as:

$$\alpha_s = 0.5 \sum_{j=1,2} (\rho_{(dir,j)} f_b + \rho_{(dif,j)}(1 - f_b)) \tag{A1}$$

where f_b is the fraction of direct beam shortwave radiation and $\rho_{(dir,j)}$ and $\rho_{(dif,j)}$ are the effective combined soil and canopy reflectance for direct and diffuse radiation in the VIS ($j = 1$) and NIR ($j = 2$) spectral bands.

The effective combined canopy reflectances ($\rho_{(dir,j)}$ and $\rho_{(dif,j)}$) in each band in Eq. A1 are defined as:

$$\begin{aligned}\rho_{(dir,j)} = {} & \rho_{(can\_dir,j)} \\ & + (\rho_{(soil,j)} - \rho_{(can\_dir,j)}) \exp(-2k^*_{(dir,j)}\Lambda)\end{aligned} \tag{A2}$$

$$\begin{aligned}\rho_{(dif,j)} = {} & \rho_{(can\_dif,j)} \\ & + (\rho_{(soil,j)} - \rho_{(can\_dif,j)}) \exp(-2k^*_{(dif,j)}\Lambda)\end{aligned} \tag{A3}$$

where $\rho_{(can\_dir,j)}$ and $\rho_{(can\_dif,j)}$ is the canopy reflectance for direct and diffuse radiation, $\rho_{(soil,j)}$ is the soil reflectance, $k^*_{(dir,j)}$ and $k^*_{(dif,j)}$ are the extinction coefficients for direct and diffuse radiation, and Λ the LAI.

The canopy direct and diffuse reflectance ($\rho_{(can\_dir,j)}$ and $\rho_{(can\_dif,j)}$) in each band in Eqs. A2 and A3 are defined as:

$$\rho_{(can\_dir,j)} = \frac{2k_{dir}}{k_{dir}+k_{dif}}\rho_{(can\_black,j)} \tag{A4}$$

$$\rho_{(can\_dif,j)} = 2\int_0^{\frac{\pi}{2}} \rho_{(can\_dir,j)} \sin(\theta)\cos(\theta)d\theta \tag{A5}$$

where k_{dir} and k_{dif} are the extinctions coefficient for a canopy with black leaves for direct and diffuse radiation, $\rho_{(can\_black,j)}$ is the reflectance of a horizontally homogeneous canopy with horizontal black leaves, and θ is the solar zenith angle.

The extinction coefficients for a real canopy (k^*_{dir} and k^*_{dif}) in Eqs. A2 and A3 and black canopy (k_{dir} and k_{dif}) in Eqs. A4 and A5, are related as follows (Goudriaan and van Laar, 1994):

$$k^*_{(dir,j)} = k_{dir}(1-\omega_j)^{\frac{1}{2}} \ , \ k^*_{(dif,j)} = k_{dif}(1-\omega_j)^{\frac{1}{2}} \tag{A6}$$

where ω_j is the scattering coefficient for each waveband is equal to the sum of the canopy reflectance and transmittance.

The extinction coefficients for a black canopy (k_{dir} and k_{dif}) in Eqs. A4 and A5 are defined as:

$$k_{dir}(\theta) = \frac{G}{\cos(\theta)} \tag{A7}$$

$$k_{dif} = -\frac{1}{\Lambda}\ln\left[\int_0^{\Lambda} \exp(-k_{dir}(\theta)\lambda)d\lambda\right] \tag{A8}$$

where λ is the cumulative canopy LAI from the canopy top and G is the ratio of the projected area of leaves in the direction perpendicular to the direction of incident solar radiation and the

actual leaf area:

$$G = \phi_1 + \phi_2 \cos(\theta), \tag{A9}$$

$$\phi_1 = 0.5 - \chi(0.633 + 0.33\chi), \tag{A10}$$

$$\phi_2 = 0.877(1 - 2\phi_1) \tag{A11}$$

where χ is an empirical parameter related to the leaf angle distribution applicable over the range [-0.4,0.6].

Finally, the reflectance of a horizontally homogeneous canopy with horizontal black leaves ($\rho_{(can\_black,j)}$) in Eq. A4 is defined as:

$$\rho_{(can\_black,j)} = \frac{1 - (1 - \omega_j)^{\frac{1}{2}}}{1 + (1 - \omega_j)^{\frac{1}{2}}} \tag{A12}$$

Acknowledgements. All the authors except David Mocko, Crystal B. Schaaf, and Qingsong Sun are supported by the Australian Research Council Centre of Excellence for Climate System Science (CE110001028). This work was also supported by the NSW Environment Trust (RM08603). We thank CSIRO and the Bureau of Meteorology through the Center for Australian Weather and Climate Research for their support in the use of the CABLE model. We thank the National Computational Infrastructure at the Australian National University, an initiative of the Australian Government, for access to supercomputer resources. We thank the NASA GSFC LIS team for support in coupling CABLE to LIS. The MODIS derived background soil albedo was provided by Peter R. J. North from the Department of Geography, Swansea University, Swansea, United Kingdom. The modified MODIS LAI data was provided by Hua Yuan from from the Land-Atmosphere Interaction Research Group at Beijing Normal University. The AMSR-E soil moisture data was provided by Yi Liu from the University of New South Wales. The SPOT albedo product was obtained from: http://www.geoland2.eu/index.jsp, and we formally acknowledge use of SPOT albedo as per the data policy: "The research leading to these results has received funding from the European Community's Seventh Framework Program (PF7/2007-2013) under grant agreement n°218795. The BioPar SPOT/VEGETATION albedo products were originally defined in the framework of the PF5/CYCLOPES project. They are a joint property of CNES and VITO under copyright geoland2. They have been generated from the SPOT VEGETATION data under copyright Cnes and distributed by VITO". All of this assistance is gratefully acknowledged.

References

Abramowitz, G., Leuning, R., Clark, M., and Pitman, A.: Evaluating the Performance of Land Surface Models, Journal of Climate, 21, 5468–5481, 2008.

Avila, F. B., Pitman, A. J., Donat, M. G., Alexander, L. V., and Abramowitz, G.: Climate model simulated changes in temperature extremes due to land cover change, J. Geophys. Res., 117, D04 108, 2012.

Bonan, G.: Ecological climatology, Cambridge University Press, 2nd edn., 2008.

Cruz, F. T., Pitman, A. J., and Wang, Y.-P.: Can the stomatal response to higher atmospheric carbon dioxide explain the unusual temperatures during the 2002 Murray-Darling Basin drought?, J. Geophys. Res., 115, D02 101, 2010.

Davidson, A. and Wang, S.: The effects of sampling resolution on the surface albedos of dominant land cover types in the North American boreal region, Remote Sensing of Environment, 93, 211 – 224, 2004.

Decker, M., Pitman, A. J., and Evans, J. P.: Groundwater constraints on simulated transpiration variability over Southeastern Australian forests, Journal of Hydrometeorology, in press, 2012.

Dickinson, R. E.: Land surface processes and climate-surface albedos and energy balance, Advances in Geophysics, 25, 305–353, 1983.

Dickinson, R. E., Henderson-Sellers, A., and Kennedy, P. J.: Biosphere-Atmosphere Transfer Scheme (BATS) Version 1e as coupled to the NCAR Community Model, NCAR Tech. Note, NCAR/TN-387+STR, 72 pp., Natl. Cent. Atmos. Res., Boulder, Colo., 1993.

Dickinson, R. E., Shaikh, M., Bryant, R., and Graumlich, L.: Interactive Canopies for a Climate Model, Journal of Climate, 11, 2823–2836, 1998.

Disney, M., Lewis, P., Thackrah, G., Quaife, T., and Barnsley, M.: Comparison of MODIS broadband albedo over an agricultural site with ground measurements and values derived from Earth observation data at a range of spatial scales, International Journal of Remote Sensing, 25, 5297–5317, 2004.

Exbrayat, J.-F., Pitman, A. J. J., Abramowitz, G., and Wang, Y.-P.: Sensitivity of net ecosystem exchange and heterotrophic respiration to parameterization uncertainty, J. Geophys. Res., 2012.

Goudriaan, J. and van Laar, H. H.: Modelling crop growth processes, Kluwer, Amsterdam, The Netherlands, 1994.

Hirsch, A. L., Kala, J., Pitman, A. J., Carouge, C., Evans, J. P., Haverd, V., and Mocko, D.: Impact of Land Surface Initialization Approach on Subseasonal Forecast Skill: A Regional Analysis in the Southern Hemisphere, Journal of Hydrometeorology, 15, 300–319, 2014.

Houldcroft, C. J., Grey, W. M. F., Barnsley, M., Taylor, C. M., Los, S. O., and North, P. R. J.: New Vegetation Albedo Parameters and Global Fields of Soil Background Albedo Derived from MODIS for Use in a Climate Model, Journal of Hydrometeorology, 10, 183–198, 2009.

Idso, S. B., Jackson, R. D., Reginato, R. J., Kimball, B. A., and Nakayama, F. S.: The Dependence of Bare Soil Albedo on Soil Water Content, Journal of Applied Meteorology, 14, 109–113, 1975.

Jones, D., Wang, W., and Fawcett, R.: High-quality spatial climate data-sets for Australia, Australian Meteorology Magazine, 58, 233–248, 2009.

Kala, J., Decker, M., Exbrayat, J.-F., Pitman, A. J., Carouge, C., Evans, J. P., Abramowitz, G., and Mocko, D.: Influence of Leaf Area Index Prescriptions on Simulations of Heat, Moisture, and Carbon Fluxes, Journal of Hydrometeorology, 15, 489–503, 2014.

Keeling, C. D., Piper, S. C., Bacastow, R. B., Wahlen, M., Whorf, T. P., Heimann, M., and Meijer, H. A.: Atmospheric CO_2 and $^{13}CO_2$ exchange with the terrestrial biosphere and oceans from 1978 to 2000: observations and carbon cycle implications, pages 83-113, in "A History of Atmospheric CO_2 and its effects on Plants, Animals, and Ecosystems", editors, Ehleringer, J.R., T. E. Cerling, M. D. Dearing, Springer Verlag, New York, 2005.

Koster, R. D. and Milly, P. C. D.: The Interplay between Transpiration and Runoff Formulations in Land Surface Schemes Used with Atmospheric Models, Journal of Climate, 10, 1578–1591, 1997.

Koster, R. D., Guo, Z., Dirmeyer, P. A., Bonan, G., Chan, E., Cox, P., Davies, H., Gordon, C. T., Kanae, S., Kowalczyk, E., Lawrence, D., Liu, P., Lu, C.-H., Malyshev, S., McAveney, B., Mitchell, K., Mocko, D., Oki, T., Oleson, K. W., Pitman, A., Sud, Y. C., Taylor, C. M., Verseghy, D., Vasic, R., Xue, Y., and Yamada, T.: Regions of strong coupling between soil moisture and precipitation, Science, 305, 1138–1140, 2004.

Koster, R. D., Guo, Z., Yang, R., Dirmeyer, P. A., Mitchell, K., and Puma, M. J.: On the Nature of Soil Moisture in Land Surface Models, Journal of Climate, 22, 4322–4335, 2009.

Kowalczyk, E. A., Wang, Y. P., Law, R. M., Davies, H. L., McGregor, J. L., and Abramowitz, G.: The CSIRO Atmosphere Biosphere Land Exchange model for use in climate models and as an offline model. Commonwealth Scientific and Industrial Research Organisation Marine and Atmospheric Research Paper 013, November 2006, 37 pages, online accessed at: www.cmar.csiro.au/e-print/open/kowalczykea_2006a.pdf, http://www.cmar.csiro.au/e-print/open/kowalczykea_2006a.pdf, 2006.

Kumar, S., Peters-Lidard, C., Tian, Y., Houser, P., Geiger, J., Olden, S., Lighty, L., Eastman, J., Doty, B., Dirmeyer, P., Adams, J., Mitchell, K., Wood, E., and Sheffield, J.: Land information system: An interoperable framework for high resolution land surface modeling, Environmental Modelling and Software, 21, 1402 – 1415, 2006.

Kumar, S. V., Peters-Lidard, C. D., Eastman, J. L., and Tao, W.-K.: An integrated high-resolution hydrometeorological modeling testbed using LIS and WRF, Environmental Modelling and Software, 23, 169 – 181, 2008.

Lacaze, R., Makhmara, H., and Smets, B.: Towards an Operational GMES Land Monitoring Core Service BioPar Product User Manual SPOT/VEGETATION V1 (BP-05), Tech. Rep. BP-RP-BP053, 11.22, http://web.vgt.vito.be/documents/BioPar/g2-BP-RP-BP053-ProductUserManual-ALBV1.pdf, 2012.

Lawrence, P. J. and Chase, T. N.: Representing a new MODIS consistent land surface in the Community Land Model (CLM 3.0), Journal of Geophysical Research: Biogeosciences, 112, 2007.

Liang, X.-Z., Xu, M., Gao, W., Kunkel, K., Slusser, J., Dai, Y., Min, Q., Houser, P. R., Rodell, M., Schaaf, C. B., and Gao, F.: Development of land surface albedo parameterization based on Moderate Resolution Imaging Spectroradiometer (MODIS) data, Journal of Geophysical Research: Atmospheres, 110, 2005.

Liu, Y. Y., van Dijk, A. I. J. M., de Jeu, R. A. M., and Holmes, T. R. H.: An analysis of spatiotemporal variations of soil and vegetation moisture from a 29-year satellite-derived data set over mainland Australia, Water Resources Research, 45, 2009.

Lorenz, R., Pitman, A. J., Donat, M. G., Hirsch, A. L., Kala, J., Kowalczyk, E. A., Law, R. M., and Srbinovsky, J.: Representation of climate extreme indices in the ACCESS1.3b coupled atmosphere–land surface model, Geoscientific Model Development, 7, 545–567, 2014.

Lucht, W., Schaaf, C., and Strahler, A.: An algorithm for the retrieval of albedo from space using semi-empirical BRDF models, Geoscience and Remote Sensing, IEEE Transactions on, 38, 977–998, 2000.

Mao, J., Phipps, S. J., Pitman, A. J., Wang, Y. P., Abramowitz, G., and Pak, B.: The CSIRO Mk3L climate system model v1.0 coupled to the CABLE land surface scheme v1.4b: evaluation of the control climatology, Geoscientific Model Development, 4, 1115–1131, 2011.

Meng, X., Evans, J., and McCabe, M.: The influence of inter-annually varying albedo on regional climate and drought, Climate Dynamics, pp. 1–17, 2013.

Oleson, K. W., Bonan, G. B., Schaaf, C., Gao, F., Jin, Y., and Strahler, A.: Assessment of global climate model land surface albedo using MODIS data, Geophysical Research Letters, 30, 2003.

Pinty, B., Andredakis, I., Clerici, M., Kaminski, T., Taberner, M., Verstraete, M. M., Gobron, N., Plummer, S., and Widlowski, J.-L.: Exploiting the MODIS albedos with the Two-stream Inversion Package (JRC-TIP): 1. Effective leaf area index, vegetation, and soil properties, Journal of Geophysical Research: Atmospheres, 116, 2011.

Pitman, A. J., Avila, F. B., Abramowitz, G., Wang, Y. P., Phipps, S. J., and de Noblet-Ducoudré, N.: Importance of background climate in determining impact of land-cover change on regional climate, Nature Climate Change, 9, 472–475, 2011.

Raupach, M. R.: Simplified expressions for vegetation roughness length and zero-plane displacement as functions of canopy height and area index, Boundary-Layer Meteorology, 71, 211–216, 1994.

Rienecker, M. M., Suarez, M. J., Gelaro, R., Todling, R., Bacmeister, J., Liu, E., Bosilovich, M. G., Schubert, S. D., Takacs, L., Kim, G.-K., Bloom, S., Chen, J., Collins, D., Conaty, A., da Silva, A., Gu, W., Joiner, J., Koster, R. D., Lucchesi, R., Molod, A., Owens, T., Pawson, S., Pegion, P., Redder, C. R., Reichle, R., Robertson, F. R., Ruddick, A. G., Sienkiewicz, M., and Woollen, J.: MERRA: NASA's Modern-Era Retrospective Analysis for Research and Applications, Journal of Climate, 24, 3624–3648, 2011.

Schaaf, C. B., Gao, F., Strahler, A. H., Lucht, W., Li, X., Tsang, T., Strugnell, N. C., Zhang, X., Jin, Y., Muller, J.-P., Lewis, P., Barnsley, M., Hobson, P., Disney, M., Roberts, G., Dunderdale, M., Doll, C., d'Entremont, R. P., Hu, B., Liang, S., Privette, J. L., and Roy, D.: First operational BRDF, albedo nadir reflectance products from MODIS, Remote Sensing of Environment, 83, 135–148, 2002.

Spitters, C.: Separating the diffuse and direct component of global radiation and its implications for modeling canopy photosynthesis Part II. Calculation of canopy photosynthesis, Agricultural and Forest Meteorology, 38, 231 – 242, 1986.

Tsvetsinskaya, E. A., Schaaf, C. B., Gao, F., Strahler, A. H., Dickinson, R. E., Zeng, X., and Lucht, W.: Relating MODIS-derived surface albedo to soils and rock types over Northern Africa and the Arabian peninsula, Geophysical Research Letters, 29, 2002.

Vamborg, F. S. E., Brovkin, V., and Claussen, M.: The effect of a dynamic background albedo scheme on Sahel/Sahara precipitation during the mid-Holocene, Climate of the Past, 7, 117–131, 2011.

Wang, Y.-P. and Leuning, R.: A two-leaf model for canopy conductance, photosynthesis and partitioning of available energy I:: Model description and comparison with a multi-layered model, Agricultural and Forest Meteorology, 91, 89 – 111, 1998.

Wang, Y. P., Kowalczyk, E., Leuning, R., Abramowitz, G., Raupach, M. R., Pak, B., van Gorsel, E., and Luhar, A.: Diagnosing errors in a land surface model (CABLE) in the time and frequency domains, J. Geophys. Res., 116, G01 034, 2011.

Wang, Y. P., Lu, X. J., Wright, I. J., Dai, Y. J., Rayner, P. J., and Reich, P. B.: Correlations among leaf traits provide a significant constraint on the estimate of global gross primary production, Geophys. Res. Lett., 39, L19 405, 2012.

Wang, Z., Zeng, X., Barlage, M., Dickinson, R. E., Gao, F., and Schaaf, C. B.: Using MODIS BRDF and Albedo Data to Evaluate Global Model Land Surface Albedo, Journal of Hydrometeorology, 5, 3–14, 2004.

Wang, Z., Barlage, M., Zeng, X., Dickinson, R. E., and Schaaf, C. B.: The solar zenith angle dependence of desert albedo, Geophysical Research Letters, 32, 2005.

Wang, Z., Schaaf, C. B., Strahler, A. H., Chopping, M. J., Roman, M. O., Shuai, Y., Woodcock, C. E., Hollinger, D. Y., and Fitzjarrald, D. R.: Evaluation of MODIS albedo product (MCD43A) over grassland, agriculture and forest surface types during dormant and snow-covered periods, Remote Sensing of Environment, 140, 60–77, 2014.

Wei, X., Hahmann, A. N., Dickinson, R. E., Yang, Z.-L., Zeng, X., Schaudt, K. J., Schaaf, C. B., and Strugnell, N.: Comparison of albedos computed by land surface models and evaluation against remotely sensed data, Journal of Geophysical Research: Atmospheres, 106, 20 687–20 702, 2001.

Yang, F., Mitchell, K., Hou, Y.-T., Dai, Y., Zeng, X., Wang, Z., and Liang, X.-Z.: Dependence of Land Surface Albedo on Solar Zenith Angle: Observations and Model Parameterization, Journal of Applied Meteorology and Climatology, 47, 2963–2982, 2008.

Yuan, H., Dai, Y., Xiao, Z., Ji, D., and Shangguan, W.: Reprocessing the MODIS Leaf Area Index products for land surface and climate modelling, Remote Sensing of Environment, 115, 1171 – 1187, 2011.

Zaitchik, B. F., Santanello, J. A., Kumar, S. V., and Peters-Lidard, C. D.: Representation of soil moisture feedbacks during drought in NASA Unified WRF (NU-WRF), Journal of Hydrometeorology, 2012.

Zhang, Q., Wang, Y. P., Pitman, A. J., and Dai, Y. J.: Limitations of nitrogen and phosphorous on the terrestrial carbon uptake in the 20th century, Geophys. Res. Lett., 38, L22 701, 2011.

Zhou, L., Dickinson, R. E., Tian, Y., Zeng, X., Dai, Y., Yang, Z.-L., Schaaf, C. B., Gao, F., Jin, Y., Strahler, A., Myneni, R. B., Yu, H., Wu, W., and Shaikh, M.: Comparison of seasonal and spatial variations of albedos from Moderate-Resolution Imaging Spectroradiometer (MODIS) and Common Land Model, Journal of Geophysical Research: Atmospheres, 108, 2003.

Table 1. Saturated and dry soil albedos for different soil colours (Fig. 2(c)) in the VIS and NIR wavebands.

Soil	α_{sat}		α_{dry}	
Color	VIS	NIR	VIS	NIR
1	0.12	0.24	0.24	0.48
2	0.11	0.22	0.22	0.44
3	0.10	0.20	0.20	0.40
4	0.09	0.18	0.18	0.36
5	0.08	0.16	0.16	0.32
6	0.07	0.14	0.14	0.28
7	0.06	0.12	0.12	0.24
8	0.05	0.10	0.10	0.20

Table 2. Names of plant functional types (PFTs) and soil types shown in Fig. 2(a).

PFT number	PFT
1	Evergreen Needleleaf
2	Evergreen Broadleaf
3	Deciduous Needleleaf
4	Deciduous Broadleaf
5	Mixed Forest
6	Closed Shrublands
7	Open Shrublands
8	Woody Savannas
9	Savannas
10	Grasslands
11	Permanent Wetlands
12	Croplands
13	Urban and Built-up
14	Cropland Mosaics
15	Snow and Ice
16	Barren

Table 3. Root-mean-square error (RMSE) and bias (scaled by 100) between the CNTL experiment and MODIS and SPOT black-sky (Black-S) visible (VIS) and near infra-red (NIR) albedo, and MODIS blue-sky (Blue-S) VIS and NIR albedo at yearly and seasonal time-scale.

	YEARLY		DJF		MAM		JJA		SON	
	RMSE	Bias	RMSE	Bias	RMSE	Bias	RMSE	Bias	RMSE	Bias
					MODIS					
Black-S-VIS	3.43	2.40	2.71	1.13	3.80	2.80	4.28	3.36	3.37	2.30
Black-S-NIR	7.18	-6.06	8.85	-7.86	7.11	-5.91	6.45	-4.97	6.72	-5.52
Blue-S-VIS	6.75	6.30	6.17	5.63	6.94	6.53	7.53	7.11	6.43	5.91
Blue-S-NIR	3.52	2.10	3.53	1.88	3.54	1.97	3.99	2.60	3.37	1.94
					SPOT					
Black-S-VIS	3.43	2.63	2.46	0.77	3.69	2.84	4.79	4.14	3.55	2.78
Black-S-NIR	6.69	-5.90	9.03	-8.29	7.00	-6.20	5.27	-4.11	5.96	-4.99

Table 4. Same as in Table 3 except for the PSALB experiment.

	YEARLY		DJF		MAM		JJA		SON	
	RMSE	Bias	RMSE	Bias	RMSE	Bias	RMSE	Bias	RMSE	Bias
					MODIS					
Black-S-VIS	3.40	0.64	3.37	-0.59	3.59	0.99	3.85	1.66	3.43	0.50
Black-S-NIR	9.47	-7.65	10.96	-9.38	9.44	-7.58	8.75	-6.54	9.08	-7.12
Blue-S-VIS	4.83	3.56	4.27	2.74	5.02	3.79	5.57	4.51	4.66	3.21
Blue-S-NIR	5.48	-0.45	5.56	-0.80	5.60	-0.61	5.61	0.15	5.42	-0.54
					SPOT					
Black-S-VIS	3.35	0.81	3.48	-1.02	3.53	0.97	4.12	2.37	3.42	0.90
Black-S-NIR	8.99	-7.56	11.13	-9.88	9.31	-7.93	7.57	-5.75	8.37	-6.67

Table 5. Saturated and dry soil albedos for 20-Class soil colours (Fig. 11) in the VIS and NIR wavebands.

Soil	α_{sat}		α_{dry}	
Color	VIS	NIR	VIS	NIR
1	0.25	0.50	0.36	0.61
2	0.23	0.46	0.34	0.57
3	0.21	0.42	0.32	0.53
4	0.20	0.40	0.31	0.51
5	0.19	0.38	0.30	0.49
6	0.18	0.36	0.29	0.48
7	0.17	0.34	0.28	0.45
8	0.16	0.32	0.27	0.43
9	0.15	0.30	0.26	0.41
10	0.14	0.28	0.25	0.39
11	0.13	0.26	0.24	0.37
12	0.12	0.24	0.23	0.35
13	0.11	0.22	0.22	0.33
14	0.10	0.20	0.20	0.31
15	0.09	0.18	0.18	0.29
16	0.08	0.16	0.16	0.27
17	0.07	0.14	0.14	0.25
18	0.06	0.12	0.12	0.24
19	0.05	0.10	0.10	0.21
20	0.04	0.08	0.08	0.16

Table 6. Same as in Table 3 except for the PSALB_20 experiment.

	YEARLY		DJF		MAM		JJA		SON	
	RMSE	Bias	RMSE	Bias	RMSE	Bias	RMSE	Bias	RMSE	Bias
					MODIS					
Black-S-VIS	2.66	-0.15	2.98	-1.40	2.87	0.23	2.95	0.91	2.67	-0.36
Black-S-NIR	10.36	-9.34	11.94	-11.07	10.31	-9.21	9.42	-8.15	9.99	-8.93
Blue-S-VIS	3.32	2.42	2.79	1.54	3.57	2.67	4.11	3.42	3.10	2.04
Blue-S-NIR	4.74	-2.91	5.2	-3.35	4.93	-3.02	4.42	-2.23	4.77	-3.05
					SPOT					
Black-S-VIS	2.57	0.0	3.2	-1.85	2.85	0.19	3.16	1.61	2.54	0.03
Black-S-NIR	9.94	-9.28	12.19	-11.61	10.27	-9.60	8.28	-7.39	9.28	-8.51

Table 7. Same as in Table 3 except for the PSALB_20C experiment.

	YEARLY		DJF		MAM		JJA		SON	
	RMSE	Bias	RMSE	Bias	RMSE	Bias	RMSE	Bias	RMSE	Bias
					MODIS					
Black-S-VIS	2.30	0.18	2.54	-1.03	2.54	0.57	2.72	1.20	2.26	-0.02
Black-S-NIR	9.52	-8.62	11.13	-10.30	9.45	-8.48	8.63	-7.51	9.12	-8.21
Blue-S-VIS	3.30	2.92	2.61	2.08	3.58	3.18	4.20	3.88	2.98	2.53
Blue-S-NIR	3.43	-1.82	3.72	-2.20	3.62	-1.91	3.42	-1.20	3.40	-1.98
					SPOT					
Black-S-VIS	2.20	0.34	2.73	-1.47	2.49	0.55	3.00	1.91	2.16	0.38
Black-S-NIR	9.10	-8.54	11.37	-10.81	9.41	-8.84	7.47	-6.74	8.40	-7.77

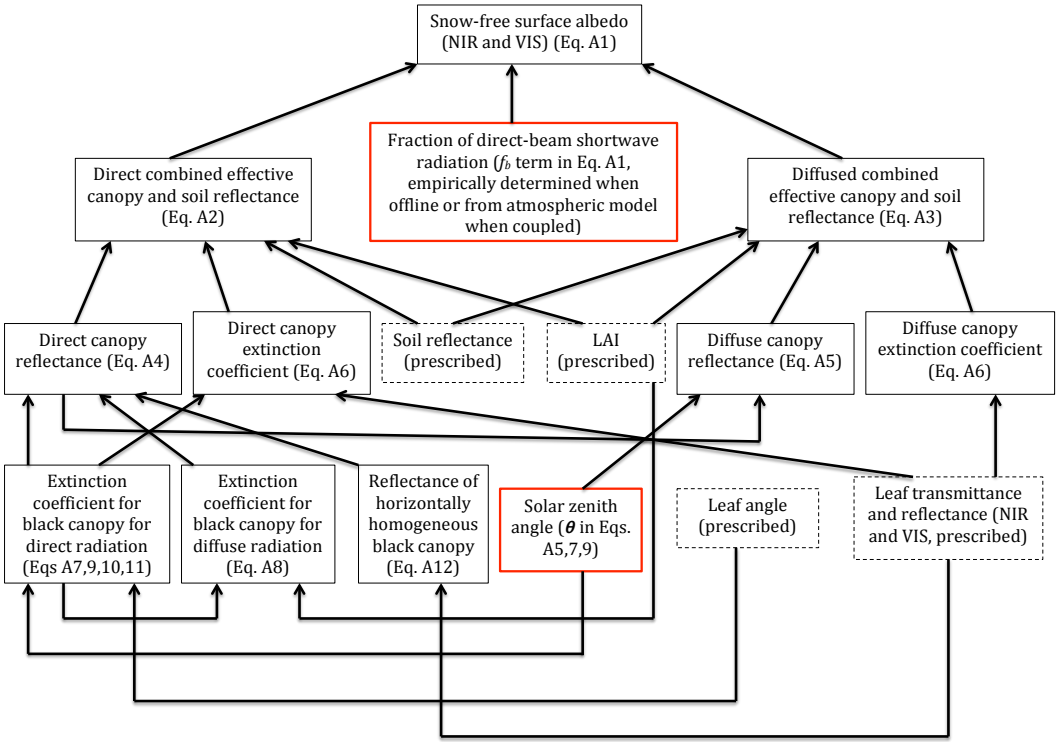

Fig. 1. Schematic illustration of snow-free surface albedo parameterisation in CABLE. Boxes with dashed lines represent user-defined input parameters to the model. The boxes with solid black lines represent the equations described in Appendix A and the boxes in solid red lines represent terms used in the equations.

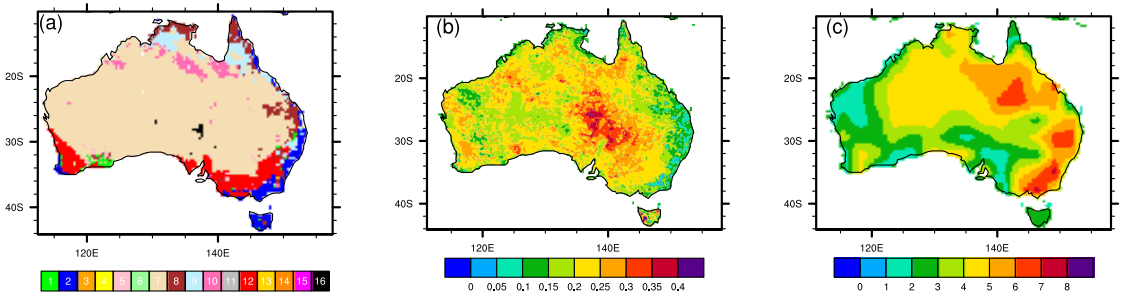

Fig. 2. (a) Distribution of PFTs in the domain, (b) prescribed background snow-free soil albedo from Houldcroft et al. (2009) used in the CNTL experiment, and (c) soil colours used in the PSALB experiment. The PFTs in panel (a) are shown in Table 2.

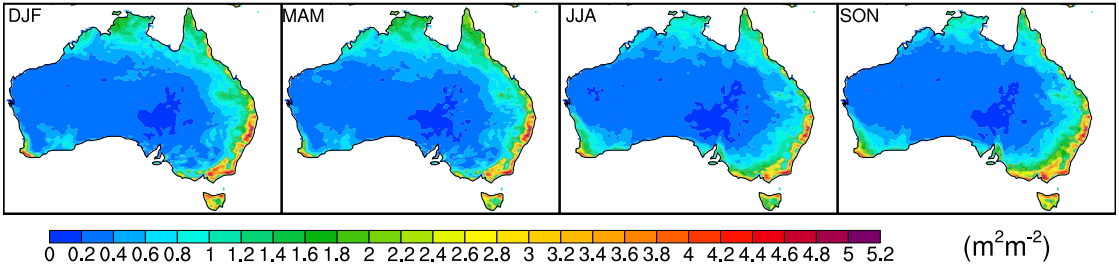

Fig. 3. Seasonal mean LAI from Yuan et al. (2011) (monthly means are used in the simulations).

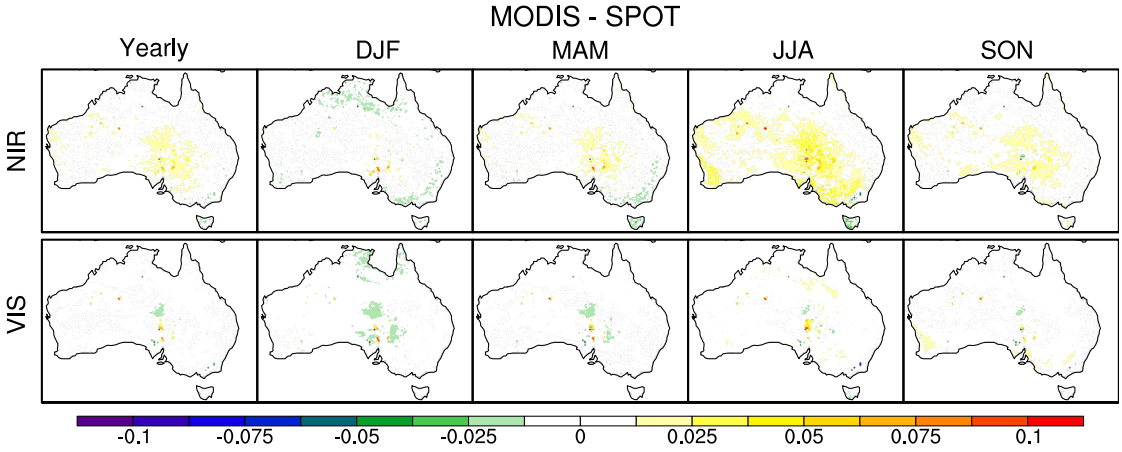

Fig. 4. Yearly and seasonal difference between MODIS and SPOT (MODIS-SPOT) VIS and NIR Black Sky albedo.

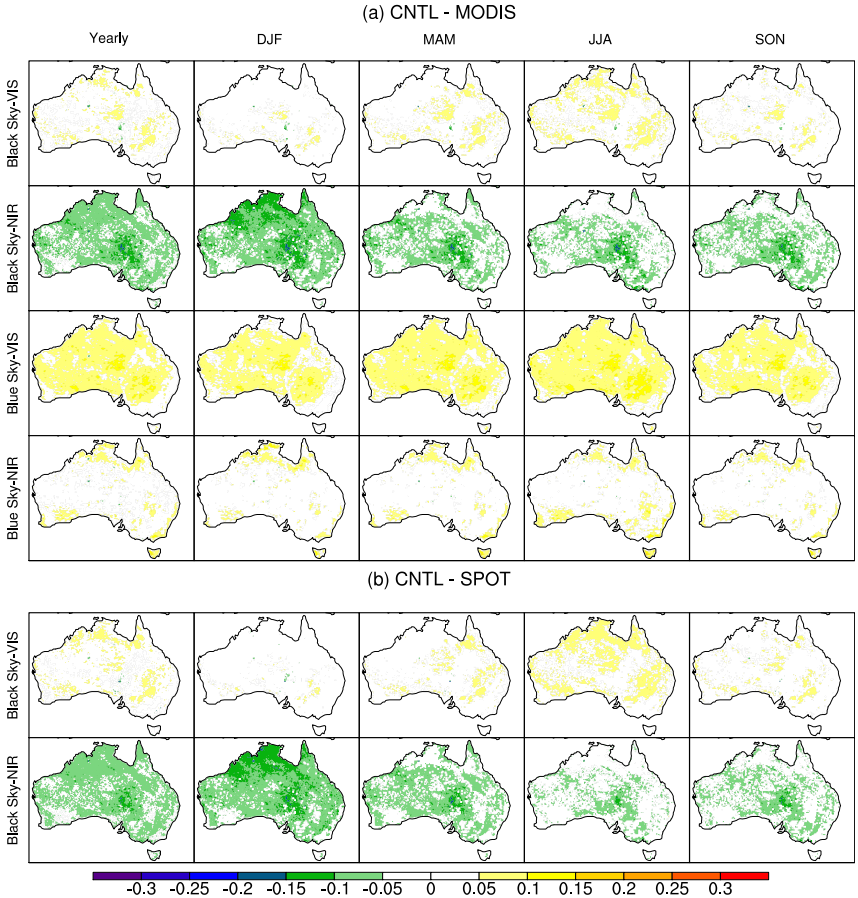

Fig. 5. Mean yearly and seasonal differences between (a) CNTL and MODIS albedo (CNTL-MODIS), and (b) CNTL and SPOT albedo (CNTL-SPOT) over the period 2001-2008. December-January-February (DJF) is summer, March-April-May (MAM) is autumn, June-July-August (JJA) is winter, September-October-November (SON) is spring.

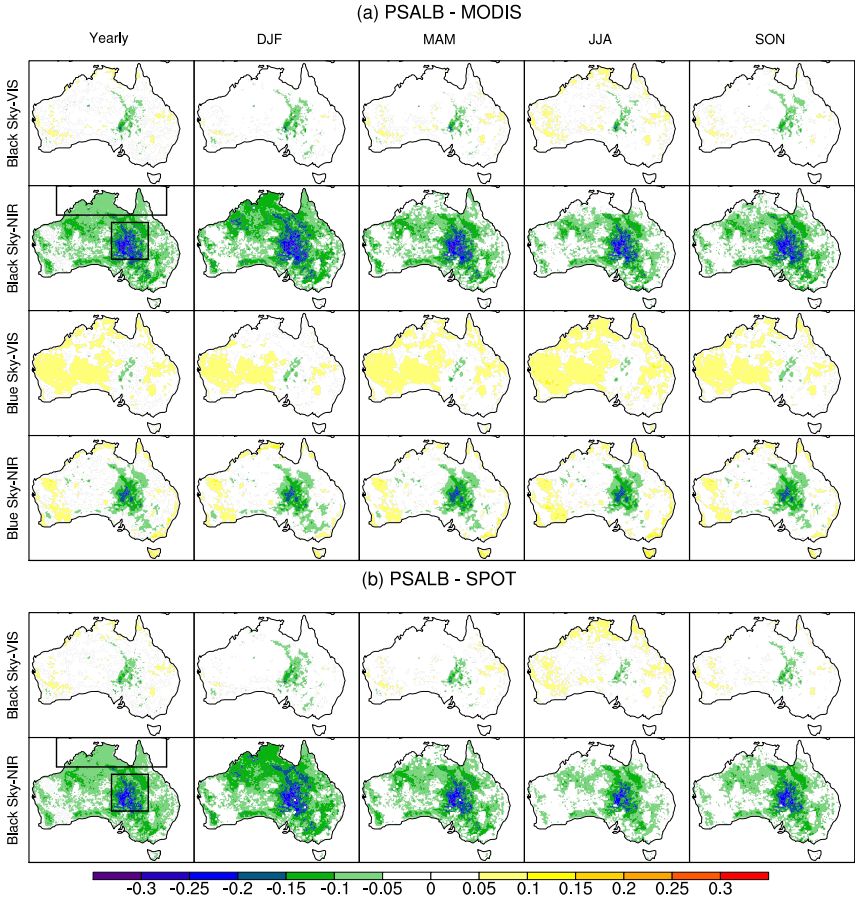

Fig. 6. Same as in Fig. 5, except for the PSALB experiment. The northern and central boxes in the Black Sky-NIR yearly panel show the regions from which a time-series is plotted in Fig. 7.

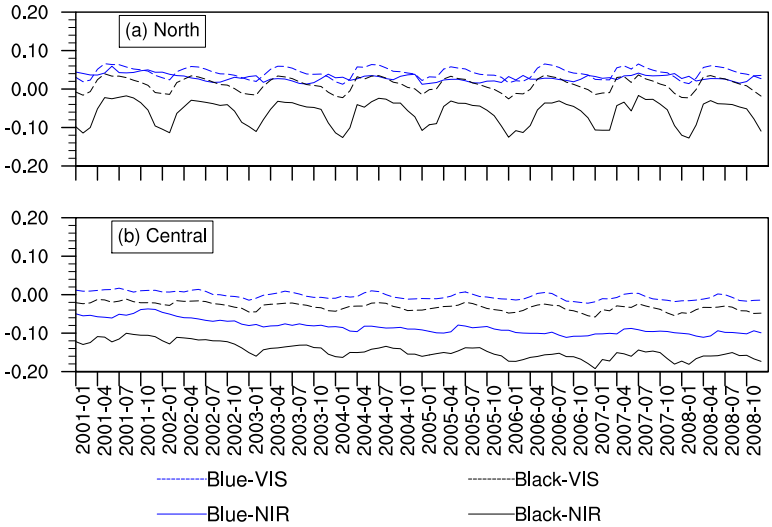

Fig. 7. Monthly time series of difference between PSALB and MODIS (PSALB-MODIS) spatially averaged over the northern and central boxes shown in the Black Sky-NIR yearly panel in Fig. 6.

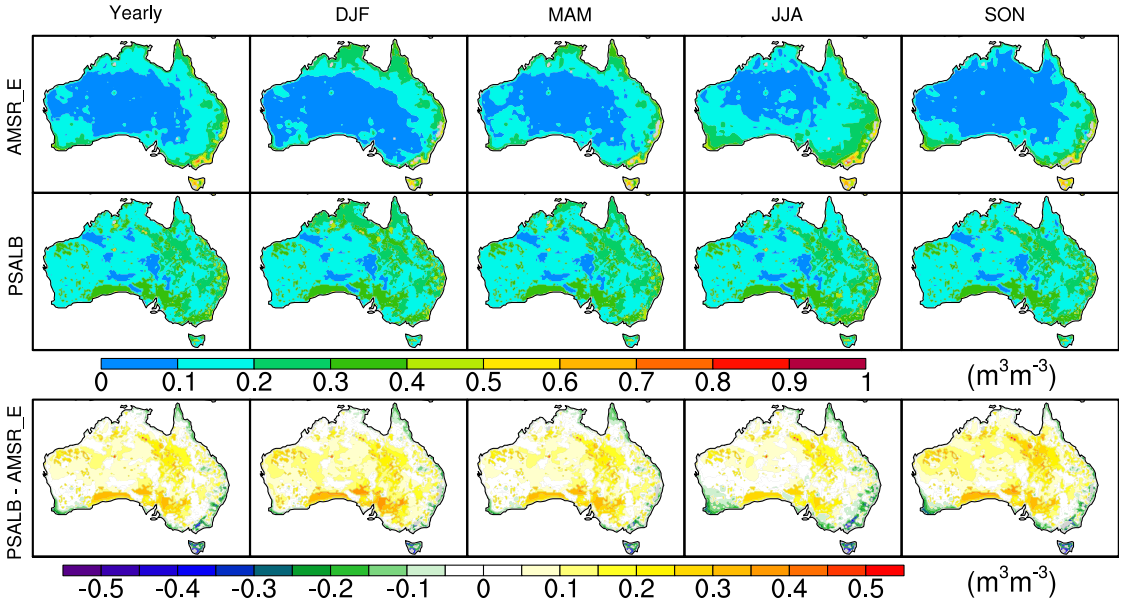

Fig. 8. Yearly and seasonal soil moisture from AMSR-E, the PSALB experiment, and difference between PSALB and AMSR-E (PSALB-AMSR_E).

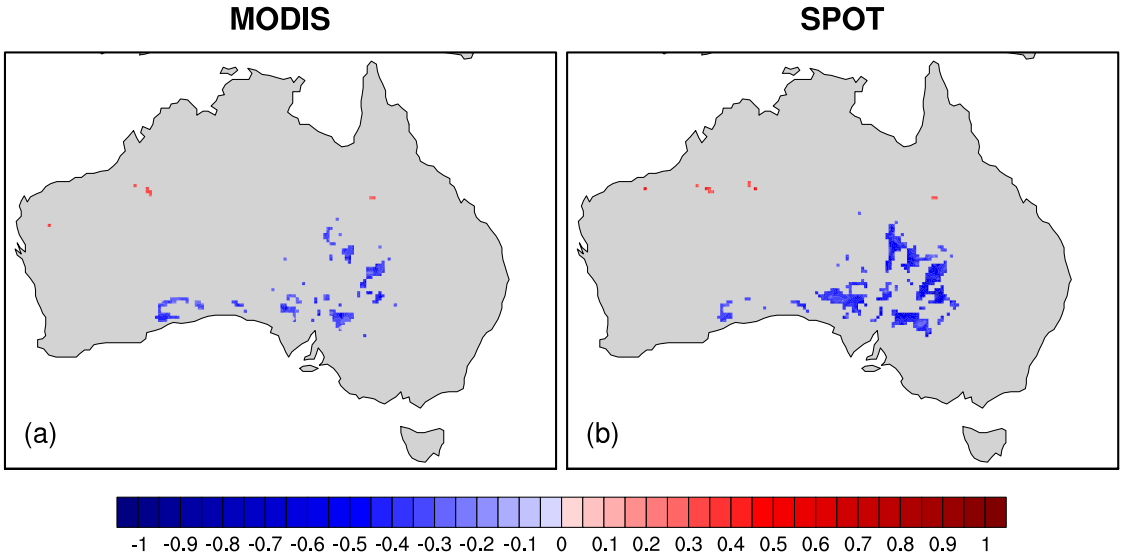

Fig. 9. Zero-lag correlation between the differences in monthly mean soil moisture between CABLE and AMSR_E (CABLE - AMSR_E) and (a) CABLE and MODIS Black-Sky NIR albedo (CABLE - MODIS), and (b) CABLE and SPOT Black-Sky NIR albedo (CABLE-SPOT). Correlations are computed at 95% significance level over a monthly time-series from 2003-2008, which corresponds to the availability of AMSR_E soil moisture.

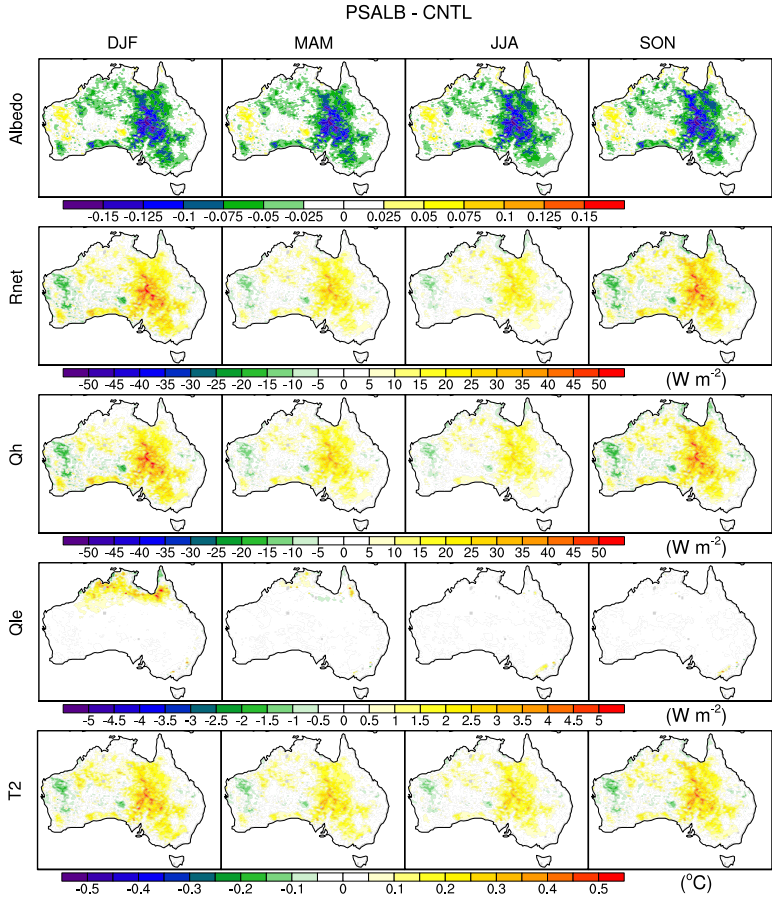

Fig. 10. Seasonal differences in albedo, net radiation (Rnet), sensible heat (Qh), latent heat (Qle) flux and screen level derived temperature (T2) between the PSALB and CNTL experiments (PSALB-CNTL).

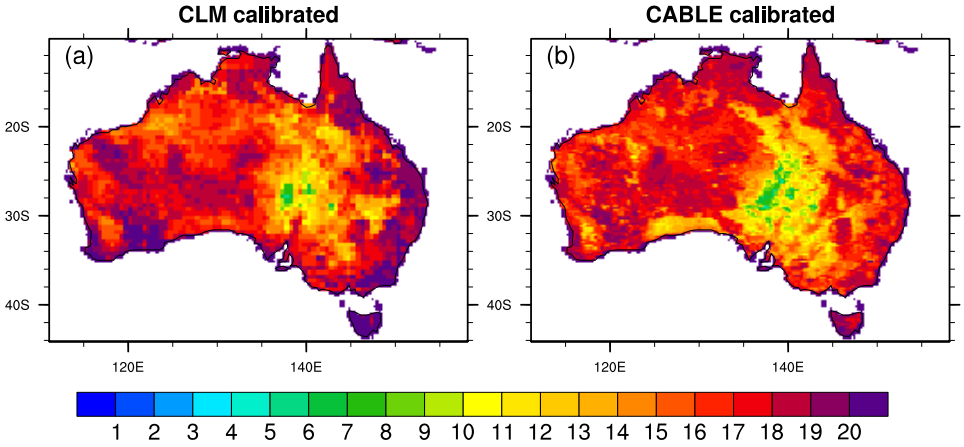

Fig. 11. 20-Class soil colour maps used for the (a) PSALB_20, and (b) PSALB_20C simulations. The corresponding saturated and dry VIS and NIR albedos for each soil colour are shown in Table 5.

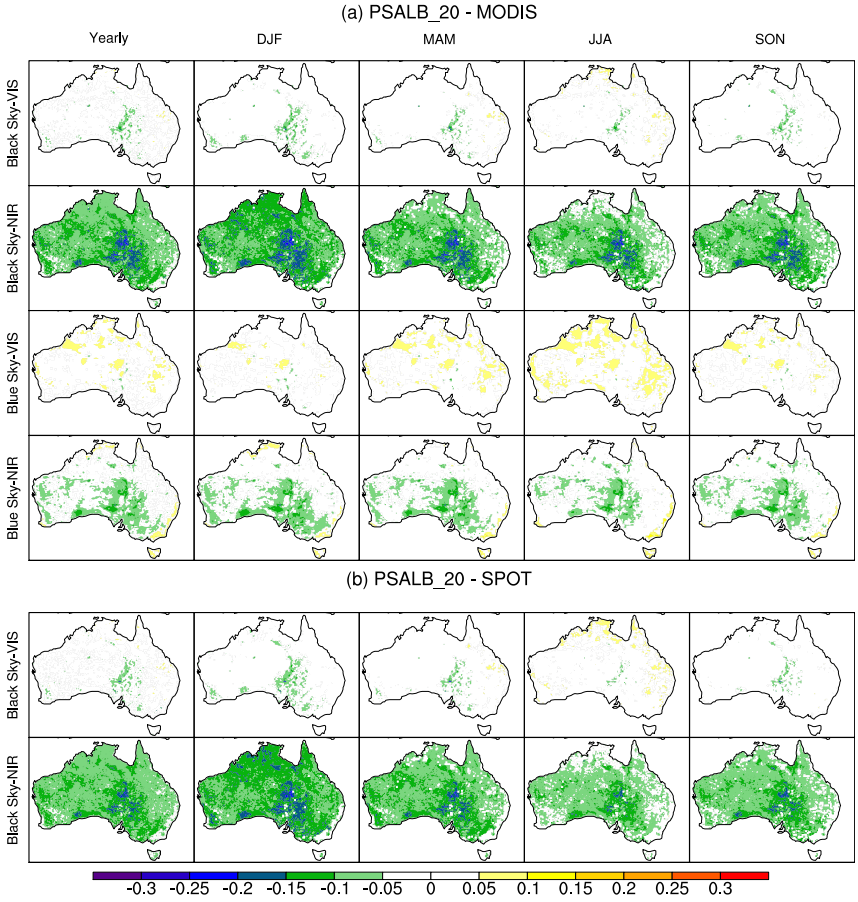

Fig. 12. Same as in Fig. 6, except for the PSALB_20 experiment.

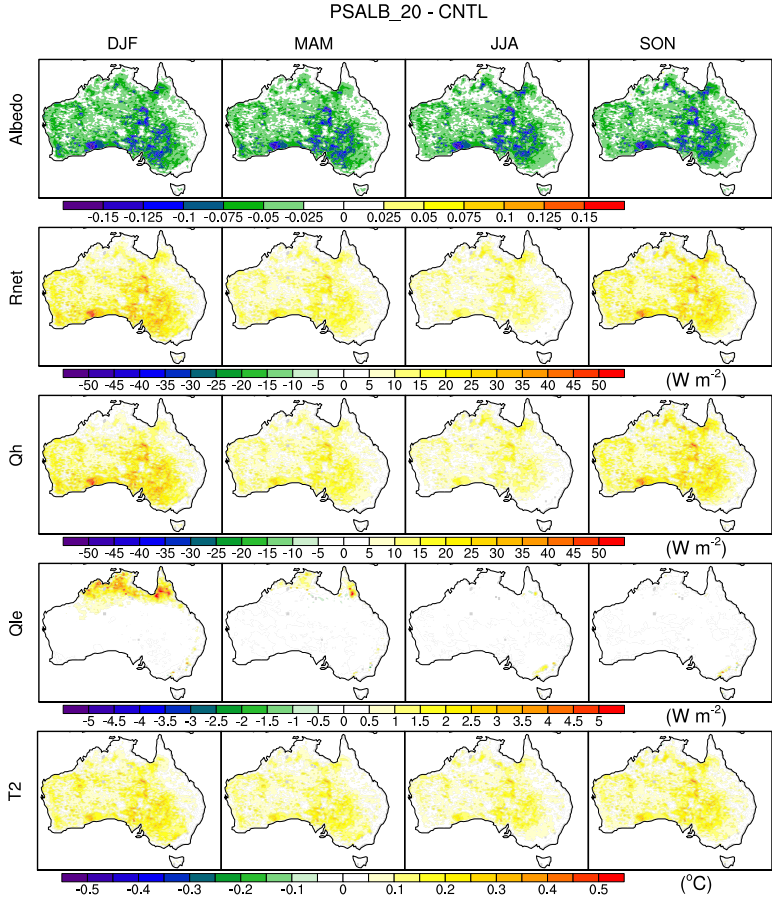

Fig. 13. Same as in Fig. 10, except for the PSALB_20 experiment.

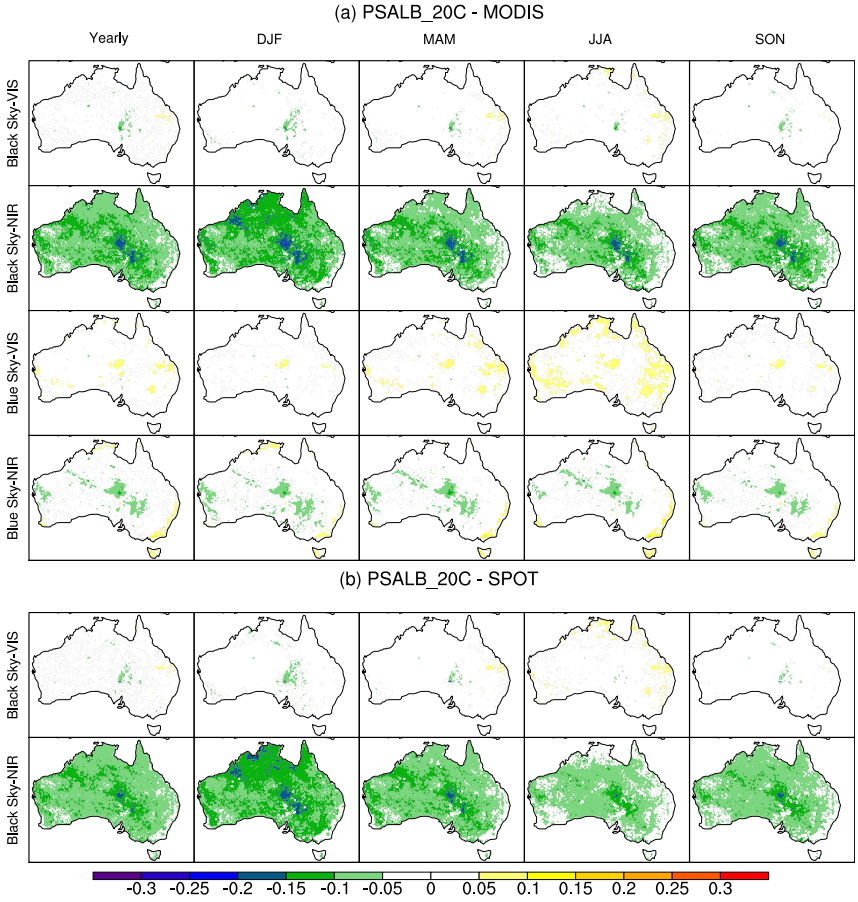

Fig. 14. Same as in Fig. 12, except for the PSALB_20C experiment.

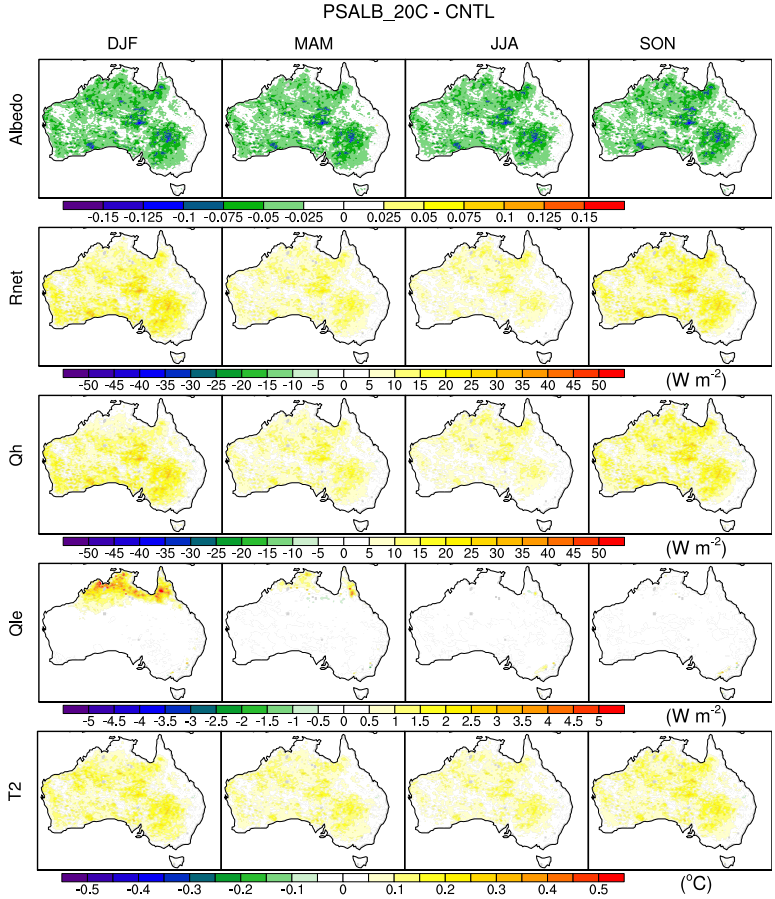

Fig. 15. Same as in Fig. 13, except for the PSALB_20C experiment.